Electron temperature in the cusp as measured with the SCIFER-2 sounding rocket

E. J. Lund,[1] M. R. Lessard,[1,2] F. Sigernes,[3] D. A. Lorentzen,[3] K. Oksavik,[3,4] P. M. Kintner,[5,6] K. A. Lynch,[7] D. H. Huang,[8] B. C. Zhang,[8] H. G. Yang,[8] and Y. Ogawa[9]

Received 23 November 2011; revised 9 March 2012; accepted 21 May 2012; published 30 June 2012.

[1] It is expected that energy deposited by soft auroral electron precipitation in the ionosphere should result in heating of ionospheric electrons in that location, and this heating is an important step in the ion outflow process. We present coordinated observations from the SCIFER-2 sounding rocket in the cusp region overflying optical observing sites in Svalbard. The rocket payload included a sensor which is designed to measure the temperature of thermal electrons. We show that elevated electron temperatures measured in situ are correlated with electron precipitation as inferred from auroral emissions during the 60–120 s preceding the passage of the rocket. This integrated "cooking time" is an important factor in determining the origin and resulting flux of outflowing ions.

Citation: Lund, E. J., et al. (2012), Electron temperature in the cusp as measured with the SCIFER-2 sounding rocket, *J. Geophys. Res.*, *117*, A06326, doi:10.1029/2011JA017404.

1. Introduction

[2] The temperature of ionospheric plasma is a notoriously difficult measurement to make. Incoherent scatter radars can measure temperatures at lower altitudes (up to ~500 km when solar activity is low), but the need to accumulate sufficient signal limits the available temporal and spatial resolution. At higher altitudes, in situ measurements are necessary. However, traditional particle detectors can fail to return useful data because spacecraft often charge to a voltage such that $|qV|$ (where q is the particle charge and V is the potential difference between the spacecraft and the surrounding plasma) is comparable to or larger than the thermal energy of the plasma. Most in situ measurements of electron temperature are obtained from Langmuir probes via a relation originally derived by *Druyvesteyn* [1930]. Among the satellite missions of the last forty years to make such measurements in the high-latitude ionosphere are the Atmospheric Explorer missions [*Brace et al.*, 1973], ESRO-1A [*Clark et al.*, 1973], Dynamics Explorer-2 [*Curtis et al.*, 1982], Ohzora [*Oyama et al.*, 1985], Akebono [*Abe et al.*, 1990], and CHAMP [*Reigber et al.*, 2002]. There have also been a handful of sounding rockets which have measured electron temperatures, such as SCIFER-1 [*Pollock et al.*, 1996].

[3] Many measurements have found that temperatures are anisotropic, with $T_{e\|} > T_{e\perp}$ (see reviews by *Demars and Schunk* [1987] and *Oyama and Schlegel* [1988]. In the auroral region this anisotropy is observed even at altitudes below 1000 km where the plasma becomes highly collisional [*Clark et al.*, 1973; *Oyama and Abe*, 1987; *Ogawa et al.*, 2000]. Subsequent modeling [*Watanabe et al.*, 1989] showed that this anisotropy can arise when parallel electric fields or a nonzero heat flux is present.

[4] At auroral and cusp latitudes, the electron temperature often responds to field-aligned currents (FACs). *Abe et al.* [1991, 1993] found that electron temperatures increase in upward FACs at all altitudes covered in their study, but in downward FACs the electron temperature decreases at higher altitudes and is not significantly affected at lower altitudes. These localized effects are not well captured in global ionospheric models such as the International Reference Ionosphere [*Liu et al.*, 2007], though it has been suggested that this defect can be overcome with more realistic convection patterns driving the ionosphere [*Crowley et al.*, 2010]. *Abe et al.* [1993] note that Joule heating is efficient at low altitudes, while the effects of particle precipitation become more important at higher altitudes. These effects, however, are not sufficient to account for observed heating at altitudes above 800 km, where nonlocal wave heating [*Curtis et al.*, 1982, 1985] and anomalous transport effects [*Zhang et al.*, 2003] become important.

[5] That ionospheric electrons are heated in regions of upward FACs suggests that precipitating electrons may be

[1]Space Science Center, University of New Hampshire, Durham, New Hampshire, USA.
[2]Department of Physics, University of New Hampshire, Durham, New Hampshire, USA.
[3]University Centre in Svalbard, Longyearbyen, Norway.
[4]Now at Department of Physics and Technology, University of Bergen, Bergen, Norway.
[5]School of Electrical and Computer Engineering, Cornell University, Ithaca, New York, USA.
[6]Deceased 16 November 2010.
[7]Department of Physics and Astronomy, Dartmouth College, Hanover, New Hampshire, USA.
[8]Polar Research Institute of China, Shanghai, China.
[9]National Institute of Polar Research, Tokyo, Japan.

Corresponding author: E. J. Lund, Space Science Center, University of New Hampshire, 8 College Rd., Durham, NH 03824, USA. (eric.lund@unh.edu)

0148-0227/12/2011JA017404

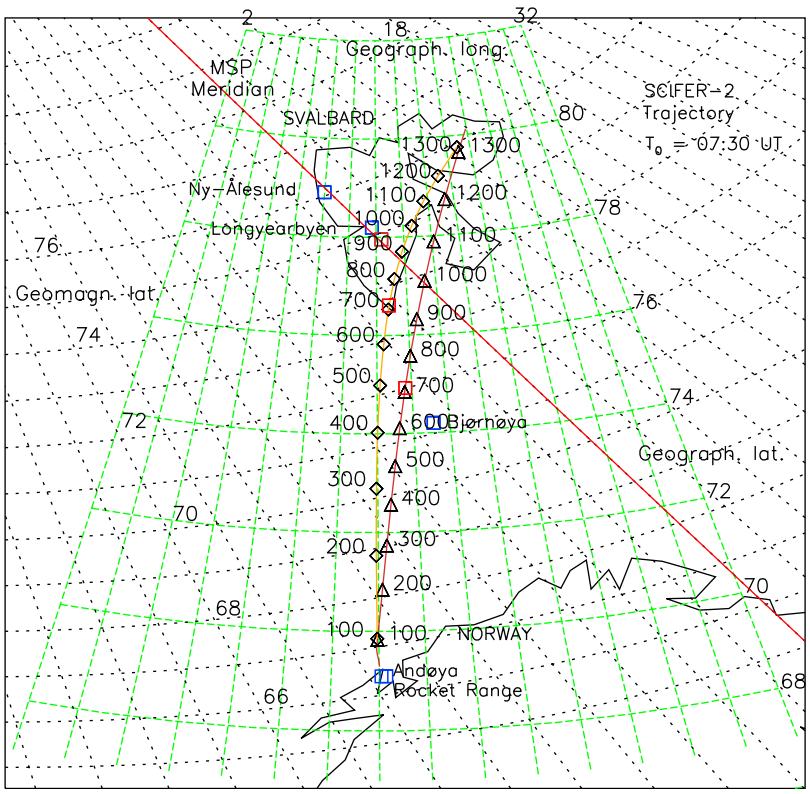

Figure 1. Trajectory of the SCIFER-2 sounding rocket: ground path (brown line) and magnetically mapped to 200 km (beige line).

the energy source for this heating. The resulting increase in electron scale height leads to an ambipolar electric field which pulls ions upward into the region where wave heating can act (see *André and Yau* [1997] for a review). In addition, small-scale FACs are correlated with observed neutral density enhancements in the topside ionosphere [*Lühr et al.*, 2004; *Sadler et al.*, 2012] and depletions at lower altitudes [*Clemmons et al.*, 2008]. This increase in scale heights means more ions are available to be accelerated into ion conics. Thus electron precipitation is one of the key causal pathways by which ion outflow occurs [*Ogawa et al.*, 2003; *Strangeway et al.*, 2005], the other being Poynting flux of Alfvén waves into the ionosphere [e.g., *Li et al.*, 2011]. A correlation between soft electron precipitation flux and upflowing/outflowing ions has been experimentally confirmed [*Moen et al.*, 2004; *Zheng et al.*, 2005; *Burchill et al.*, 2010], and simulations of nightside sounding rocket data support a causal link [*Lynch et al.*, 2007]. Electrons in the appropriate energy range are commonly observed to precipitate in the cusp, mainly due to magnetopause reconnection [e.g., *Lockwood and Smith*, 1989; *Newell and Meng*, 1992].

[6] The timescale of the ionospheric response to magnetospheric driving is an important question which has received little attention in the literature. The low temperatures in the *F* region (typically a few tenths of an eV or less), combined with high collision rates, mean that ions and neutral atoms take a long time to respond to heating, and the relatively low thermal speeds (2.5 km/s for oxygen and 420 km/s for electrons at 1 eV) mean that heat is not transported instantaneously to higher altitudes. For example, fluid simulations designed to explain tall rays [*Otto et al.*, 2003] find that high densities of neutral O are needed in the topside ionosphere. In general a finite amount of time, which we will refer to as a cooking time, will be needed to heat the ionosphere. The long integration times required for radar measurements make experimental data scarce, although there is at least one published example [*Zettergren et al.*, 2008, Figure 10d] indicating a ~100 s cooking time for electrons at 350–400 km to heat from a background temperature of ~1000 K to a 2500–3000 K level in response to soft electron precipitation. Spacecraft cannot remain on a given field line long enough to answer the question without the help of simultaneous radar or ground-based measurements. A few simulations have addressed this question, with electron response times to soft electron precipitation ranging from a few seconds [*Zhu et al.*, 2001] to ~100 s [*Zettergren et al.*, 2008; *Sadler et al.*, 2012].

[7] That cooking times for electrons should be ~100 s agrees with an order-of-magnitude estimate of energy input for precipitating electrons. Consider an ionosphere with an electron density of $\sim 10^{11}$ m^{-3} and a neutral density of $\sim 10^{14}$ m^{-3} (these are typical numbers for altitudes of ~300 km). Assume an incident energy flux of precipitating soft electrons of ~1 mW/m^2, which is the threshold for causing visible aurora, and that this energy flux is absorbed by neutrals and ionospheric electrons in proportion to their number density. Thus the electrons are heated at $\sim 10^{-6}$ W/m^2. To heat a column of electrons ~100 km in height by ~1000 K requires an energy input of $\sim 10^{-4}$ J/m^2, which represents ~100 s of electron precipitation.

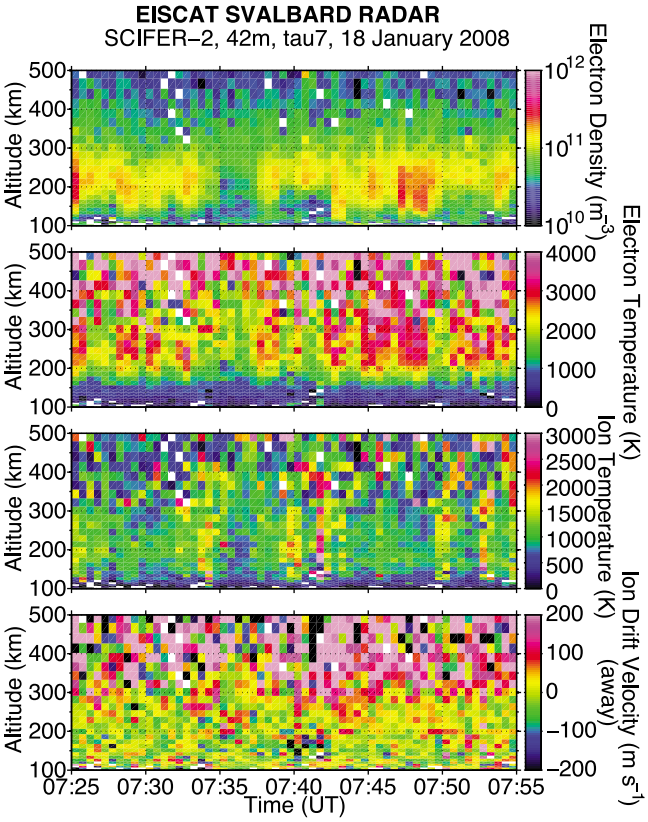

Figure 2. Ionospheric profiles from the EISCAT Svalbard Radar for 07:25–07:55 UT. (top to bottom) Electron density, electron temperature, ion temperature, and field-aligned ion drift velocity.

[8] This paper shows coordinated observations from a sounding rocket, radar, and ground-based optical instruments of an event which is consistent with the idea of a cooking time. Specifically, our data are consistent with a response time of 60–120 s for precipitating soft electrons to heat the ionosphere. We describe the instrumentation in section 2 and show the data in section 3. Our analysis is presented in section 4.

2. Instrumentation

[9] The SCIFER-2 (Sounding of the Cleft Ion Fountain Energization Region) sounding rocket was launched on 18 January 2008 at 07:30 UT from Andøya, Norway, to an apogee of 1468 km. The rocket passed over Svalbard along the trajectory shown in Figure 1. During the flight it passed through a series of poleward moving auroral forms (PMAFs) [*Sandholt et al.*, 1986, 1993], which are known to be closely related to ion upflow events in the cusp [*Moen et al.*, 2004]. The payload included electric field sensors for DC, ELF, VLF and HF electric fields; a science grade magnetometer; energetic electron and thermal and mid-energy ion detectors; and an electron retarding potential analyzer (ERPA) [*Frederick-Frost et al.*, 2007].We will focus on data from the last of these instruments.

[10] The region over Svalbard is covered by several ground-based instruments, including the EISCAT Svalbard Radar (ESR; http://eiscat.se/) and the Kjell Henriksen Observatory (KHO; http://kho.unis.no/) at Longyearbyen (78.1°N 16.0°E; 74.7° geomagnetic), and the Arctic Yellow River Station (AYRS) at Ny Ålesund (78.9°N 11.9°E; 75.8° geomagnetic). KHO is owned by the University Centre in Svalbard (UNIS), and AYRS is owned by the Polar Research Institute of China (PRIC). KHO at Longyearbyen operated a meridian scanning photometer and a white light all-sky camera. AYRS at Ny Ålesund operated an all-sky camera (ASC) system with filters covering the 427.8, 557.7, and 630.0 nm lines; these cameras record images every 10 s, including 7 s of exposure time and 3 s of readout time [*Hu et al.*, 2009]. Noon MLT at both sites is approximately 08:30 UT.

3. Presentation of Data

[11] Figure 2 shows height profiles of electron density, electron temperature, ion temperature, and field-aligned ion drift velocity as measured by the ESR antennae for the period 07:25–07:55 UT. The data was acquired using an alternating code experiment called tau7, which is optimized to monitor the topside ionosphere (data collection from 40 to 1500 km altitude), with 6 s initial time integration and spatial resolution down to 1–18 km. The raw data was then post-integrated for 30 s, in order to obtain the profiles presented in Figure 2. When SCIFER-2 passed over of Svalbard around 07:38–07:53 UT, the ESR data is characterized by the following: (1) a peak in the electron density around 200 km altitude produced by soft electron precipitation, (2) elevated electron temperatures above 200 km altitude, (3) cold ion temperatures, and (4) persistent and enhanced upflow of ions above 250–300 km altitude. We therefore use 200 km (the altitude of maximum electron density) as the reference altitude for our mapping of the optical data. In the optical observations that follow, we focus on the 630 nm line as the proxy for energy deposition at 200 km since that line is excited by electrons which penetrate to roughly that altitude [e.g., *Semeter*, 2003]. Note that the 630 nm line has a lifetime of 110 s [*Rees*, 1989, p. 177], which affects the proper interpretation of luminosity profiles as discussed in section 4. We also see elevated electron temperatures at and above 200 km, as well as ion upflow above 300 km, after 07:42 UT.

[12] Figure 3 shows two hours of MSP data from Longyearbyen in both the 630.0 nm (top) and 557.7 nm (bottom) lines. The box marked "LAUNCH" shows the period of the rocket flight. There was a significant amount of activity over Svalbard during the latter half of the flight, when the rocket was over Svalbard, consisting of a series of PMAFs mainly south of Longyearbyen and some patches to the north.

[13] Figure 4 shows the electron temperature as measured by the rocket. At several points during the flight we see spikes in the electron temperature which are ~1000 K higher than surrounding minima. Four of those spikes, all from the latter half of the flight, are marked in the figure. We examine these peaks in greater detail below.

[14] Figure 5 shows a path keogram from the 630.0 nm ASC at Ny Ålesund. The pixels extracted from the ASC images are those through which the magnetic foot point of the rocket, mapped to 200 km with the IGRF, passed (in contrast to a standard keogram, which would be constructed by choosing a path that coincides with the local magnetic

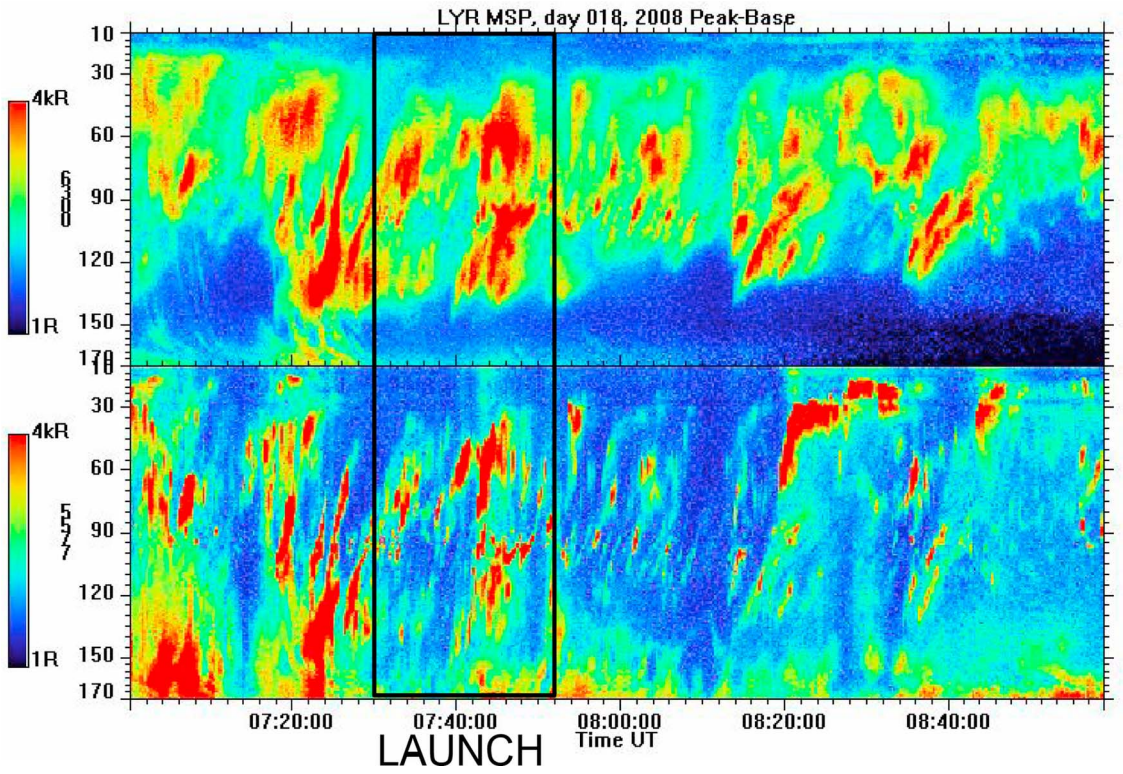

Figure 3. Meridian scanning photometer data from Longyearbyen in (top) 630.0 nm and (bottom) 557.5 nm.

meridian). The Y axis labels the pixels along the path with the time the rocket foot point traversed that pixel. There is an elevated background, mostly due to twilight, which we have not subtracted out for reasons that will be discussed in section 4. Since the rocket passed well to the south and east of Ny Ålesund, we are looking obliquely to the auroral rays, and some of the sharp features are therefore smeared out. However, we can see that the broad features of the electron temperature in Figure 4 generally correlate with the rocket's passage through auroral features visible in Figure 5, especially if the need for some nonzero cooking time is taken into account. In particular, the electron temperature increase starting just before 600 s (07:40 UT) corresponds to the first in a series of PMAFs, and the temperature increases over the next two minutes. Likewise, the decrease around 1000 s roughly corresponds to a gap between PMAFs. Note, however, that the temperature peaks marked in Figure 4 do not correspond to the luminosity peaks in Figure 5. Instead, we

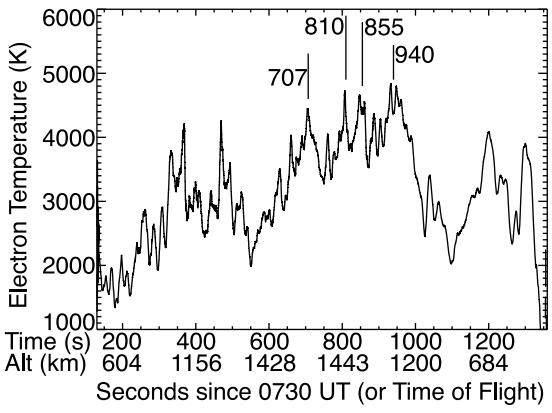

Figure 4. Electron temperature measured by the rocket as a function of time since launch. Four spikes in the temperature, which are discussed further in the text, are noted in the figure.

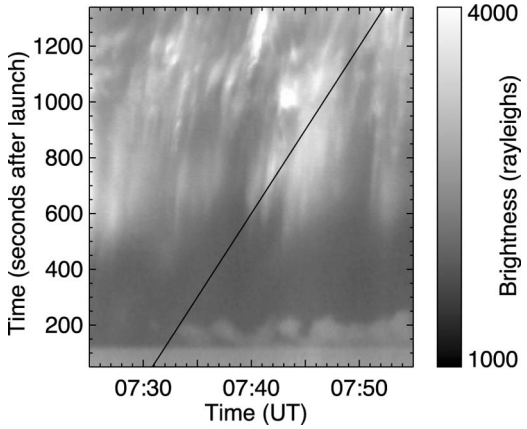

Figure 5. Path keogram extracted from the 630.0 nm ASC at Ny Ålesund. The solid diagonal line represents the real-time trajectory of the rocket's 200 km foot point. The Y axis labels the pixels along the path with the time the rocket foot point traversed that pixel. See text for a description of how this figure was constructed.

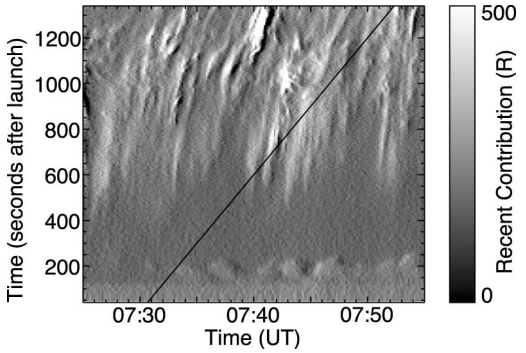

Figure 6. Path keogram showing the contribution to the measured 630.0 nm brightness due to electrons that have precipitated since the previous frame, as computed from equation (1). Format is the same as for Figure 5.

see that the rocket passed through the trailing edges of the PMAFs it encountered.

4. Analysis

[15] Because the 630 nm line has a long lifetime, the time series of intensities I_n in any given pixel includes contributions from electrons that have precipitated over a period comparable to the line lifetime, not just the instantaneous precipitation. Thus to calculate the contribution of recently precipitated electrons we model the response of the 630 nm line as a recursive filter:

$$I_n = Q_n + I_{n-1}\exp(-\Delta t/\tau) \quad (1)$$

where Q_n represents the contribution of incoming electrons and photons in the period Δt = 10 s [*Hu et al.*, 2009] since the previous frame and τ = 110 s [*Rees*, 1989] is the lifetime of the line. For a given precipitating electron spectrum in a dark ionosphere Q_n will be proportional to the precipitation rate, with the constant of proportionality strongly dependent on the details of the spectrum. At this local time there is also a contribution from dayglow, especially in the southern part of the ASC's field of view; it can be separated from the contribution due to electrons only by its much slower time variation. Of necessity (1) neglects the effects of variations on timescales shorter than the frame rate as well as statistical noise. These factors can produce spuriously negative instantaneous contributions, which occur in about 0.4% of our pixels.

[16] Solving (1) for Q_n and applying to Figure 5 yields Figure 6 as the contribution of recently precipitated electrons and photons to the 630 nm line in the pixels traversed by the rocket. This figure shows, even more so than Figure 5, that the most intense precipitation precedes the rocket passage through the auroral features. For instance, the peak at 810 s in Figure 4 falls during a gap in precipitation. Thus the observed electron temperature generally, and the temperature spikes in particular, cannot be solely due to a prompt ionospheric response to the precipitation.

[17] Figure 7 shows luminosity profiles for the ASC pixels which the rocket traverses at the four times indicated in Figures 4b–4e, as well as the deep minima in electron temperature before (panel (a)) and after (panel (f)) these four peaks. We show both I_n (solid lines, left axes) and Q_n (dotted lines, right axes) for each of these locations. The time that the rocket actually traverses the pixel is marked with a vertical line. In panel (a) we see that the luminosity remains near background levels throughout the flight, and the recent contribution is at a low steady level due to twilight photons,

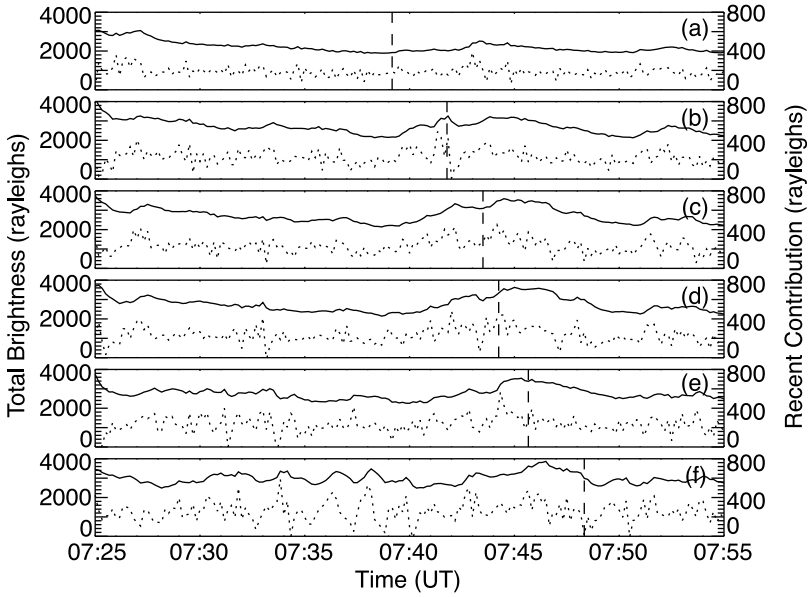

Figure 7. (left axes) Luminosity profiles (solid lines) and (right axes) the contribution thereto of recently precipitated electrons (dashed lines) of the pixels from the Ny Ålesund 630.0 nm ASC that the rocket foot point traverses at (a) 550 s, (b) 707 s, (c) 810 s, (d) 855 s, (e) 940 s, and (f) 1100 s after launch. Figures 7b–7e are the times of the four peaks marked in Figure 4, while Figures 7a and 7f align with the deep minima on either side. In each panel the time at which the rocket foot point traverses the pixel is marked with a vertical line. The Y axes give brightness in rayleighs.

so as expected the electron temperature here is low. For each of the four electron temperature peaks, we see the luminosity increases during the 2–3 minutes prior to the passage of the rocket; however, the rocket passage coincides with the peak in recent contribution for only two of these temperature peaks (panels (b) and (d)), while in panels (c) and (e) the peak contribution precedes the rocket passage by more than a minute. Thus a cooking time of less than about 60 s is incompatible with our data. In panel (f) we see a peak in the total luminosity about two minutes prior to the passage of the rocket, and the peak in the recent contribution comes even earlier. The observed luminosity at the time of the rocket passage is mainly due to the residual of earlier precipitation plus a contribution from dayglow. This point allows us to estimate an upper bound for the cooking time: it cannot be longer than about 150 s, or we should be seeing much higher electron temperatures here.

5. Discussion and Summary

[18] The data presented above suggest that soft auroral precipitation results in electron temperature enhancements in the cusp, and that some cooking time of ~100 s is required for the temperatures to increase to observed levels. This cooking time agrees with an order-of-magnitude estimate of how long it takes for precipitating electrons to contribute enough energy to produce the observed heating.

[19] This model explains the broader features of the data. The resulting increase in ionospheric scale height causes ions to be pulled upward to altitudes where the ions can be heated by plasma waves or accelerated by centrifugal effects (see *Moore and Horowitz* [2007], for a review, as well as the more recent work by *Kitamura et al.* [2010]). Our data support the idea that soft electron precipitation is a necessary condition for auroral ion outflow [*Strangeway et al.*, 2005].

[20] Because the optical data involve oblique look directions and the 630.0 nm line has a long lifetime, we do not have sufficient resolution to prove that soft auroral precipitation can explain the finer scale features in the in situ data. Joule heating may play a role in producing these fine scale structures, as has been suggested for density enhancements [*Crowley et al.*, 2010]. Note that frictional heating, which is dominated by Joule dissipation, is quadratic in the electric field (it is proportional to $\mathbf{E} \cdot \sigma \cdot \mathbf{E}$ where σ is the conductivity tensor) [e.g., *Strangeway*, 2012], so small-scale Joule heating can have a larger effect than large-scale Joule heating if the peak electric field magnitude is inversely proportional to the scale size. Fine-scale structures are difficult for global models to resolve because the scale sizes involved are frequently too small to be resolved at grid sizes practical in routine modeling, and they are of practical importance due to their occurrence in Alfvénic aurora, where most of the perpendicular ion heating is observed [*Tung et al.*, 2001; *Chaston et al.*, 2006]. The upcoming e-POP satellite mission [*Yau et al.*, 2006] may shed some further light on how soft electron precipitation and Joule heating are related to these fine scale structures.

[21] **Acknowledgments.** We thank A. Otto for helpful discussions. The work at the University of New Hampshire was supported by the National Aeronautics and Space Administration under grant NNX08AQ27G. The work at the Polar Research Institute of China was partly supported by Special Fund for Public Welfare Industry (Oceanography) (contract 201005017). The Norwegian team is supported by the Research Council of Norway and COST Action ES0803. We are indebted to the director and staff of EISCAT for operating the facility and supplying the data. EISCAT is an international association supported by research organizations in China (CRIRP), Finland (SA), France (CNRS, till end 2006), Germany (DFG), Japan (NIPR and STEL), Norway (NFR), Sweden (VR), and the United Kingdom (STFC).

[22] Robert Lysak thanks the reviewers for their assistance in evaluating this paper.

References

Abe, T., K.-I. Oyama, H. Amemiya, S. Watanabe, T. Okuzawa, and K. Schlegel (1990), Measurements of temperature and velocity distribution of thermal electrons by the Akebono (EXOS-D) satellite—Experimental setup and preliminary results, *J. Geomagn. Geoelectr.*, *42*, 537.

Abe, T., T. Okuzawa, K.-I. Oyama, H. Fukunishi, and R. Fujii (1991), Variations of thermal electron energy distribution associated with field-aligned currents, *Geophys. Res. Lett.*, *18*, 349, doi:10.1029/91GL00033.

Abe, T., K.-I. Oyama, S. Watanabe, and H. Fukunishi (1993), Characteristic features of electron temperature and density variations in field-aligned current regions, *J. Geophys. Res.*, *98*, 11,257, doi:10.1029/92JA01970.

André, M., and A. Yau (1997), Theories and observations of ion energization and outflow in the high latitude magnetosphere, *Space Sci. Rev.*, *80*, 27.

Brace, L. H., R. F. Theis, and A. Dalgarno (1973), The cylindrical electrostatic probes for Atmospheric Explorer -C, -D, and -E, *Radio Sci.*, *8*, 341, doi:10.1029/RS008i004p00341.

Burchill, J. K., D. J. Knudsen, J. H. Clemmons, K. Oksavik, R. F. Pfaff, C. T. Steigies, A. W. Yau, and T. K. Yeoman (2010), Thermal ion upflow in the cusp ionosphere and its dependence on soft electron energy flux, *J. Geophys. Res.*, *115*, A05206, doi:10.1029/2009JA015006.

Chaston, C. C., V. Genot, J. W. Bonnell, C. W. Carlson, J. P. McFadden, R. E. Ergun, R. J. Strangeway, E. J. Lund, and K. J. Hwang (2006), Ionospheric erosion by Alfvén waves, *J. Geophys. Res.*, *111*, A03206, doi:10.1029/2005JA011367.

Clark, D. H., W. J. Raitt, and A. P. Willmore (1973), A measured anisotropy in the ionospheric electron temperatures, *J. Atmos. Terr. Phys.*, *35*, 63.

Clemmons, J. H., J. H. Hecht, D. R. Salem, and D. J. Strickland (2008), Thermospheric density in the Earth's magnetic cusp as observed by the Streak mission, *Geophys. Res. Lett.*, *35*, L24103, doi:10.1029/2008GL035972.

Crowley, G., D. J. Knipp, K. A. Drake, J. Lei, E. Sutton, and H. Lühr (2010), Thermospheric density enhancements in the dayside cusp region during strong B_Y conditions, *Geophys. Res. Lett.*, *37*, L07110, doi:10.1029/2009GL042143.

Curtis, S. A., W. R. Hoegy, L. H. Brace, N. C. Maynard, M. Sugiura, and J. D. Winningham (1982), DE-2 cusp observations: Role of plasma instabilities in topside ionospheric heating and density fluctuations, *Geophys. Res. Lett.*, *9*, 997, doi:10.1029/GL009i009p00997.

Curtis, S. A., W. R. Hoegy, L. H. Brace, and J. D. Winningham (1985), Cusp altitudinal electron temperature gradient: Dynamics Explorer 2 implications for heating mechanisms, *J. Geophys. Res.*, *90*, 4415, doi:10.1029/JA090iA05p04415.

Demars, H. G., and R. W. Schunk (1987), Temperature anisotropies in the terrestrial ionosphere and plasmasphere, *Rev. Geophys.*, *25*, 1659, doi:10.1029/RG025i008p01659.

Druyvesteyn, M. J. (1930), Der Niedervoltbogen, *Z. Phys.*, *64*, 781.

Frederick-Frost, K. M., K. A. Lynch, P. M. Kintner, E. Klatt, D. Lorentzen, J. Moen, Y. Ogawa, and M. Widholm (2007), SERSIO: Svalbard EISCAT rocket study of ion outflows, *J. Geophys. Res.*, *112*, A08307, doi10.1029/2006JA011942.

Hu, Z.-J., et al. (2009), Synoptic distribution of dayside aurora: Multiple-wavelength all-sky observation at Yellow River Station in Ny-Ålesund, Svalbard, *J. Atmos. Solar Terr. Phys.*, *71*, 794, doi:10.1016/j.jastp.2009.02.010.

Kitamura, N., et al. (2010), Observations of very-low-energy (<10 eV) ion outflows dominated by O^+ ions in the region of enhanced electron density in the polar cap magnetosphere during geomagnetic storms, *J. Geophys. Res.*, *115*, A00J06, doi:10.1029/2010JA015601.

Li, W., D. Knipp, J. Lei, and J. Raeder (2011), The relation between dayside local Poynting flux enhancement and dayside reconnection, *J. Geophys. Res.*, *116*, A08301, doi:10.1029/2011JA016566.

Liu, H., C. Stolle, S. Watanabe, T. Abe, M. Rother, and D. L. Cooke (2007), Evaluation of the IRI model using CHAMP observations in polar and equatorial regions, *Adv. Space Res.*, *39*, 904, doi:10.1016/j.asr.2006.08.006.

Lockwood, M., and M. F. Smith (1989), Low-altitude signatures of the cusp and flux transfer events, *Geophys. Res. Lett.*, *16*, 879, doi:10.1029/GL016i008p00879.

Lühr, H., M. Rother, W. Köhler, P. Ritter, and L. Grunwaldt (2004), Thermospheric up-welling in the cusp region: Evidence from CHAMP observations, *Geophys. Res. Lett.*, *31*, L06805, doi:10.1029/2003GL019314.

Lynch, K. A., J. L. Semeter, M. Zettergren, P. Kintner, R. Arnoldy, E. Klatt, J. LaBelle, R. G. Michell, E. A. MacDonald, and M. Samara (2007), Auroral ion outflow: Low altitude energization, *Ann. Geophys.*, *25*, 1967, doi:10.5194/angeo-25-1967-2007.

Moen, J., K. Oksavik, and H. C. Carlson (2004), On the relationship between ion upflow events and cusp auroral transients, *Geophys. Res. Lett.*, *31*, L11808, doi:10.1029/2004GL020129.

Moore, T. E., and J. L. Horwitz (2007), Stellar ablation of planetary atmospheres, *Rev. Geophys.*, *45*, RG3002, doi:10.1029/2005RG000194.

Newell, P. T., and C.-I. Meng (1992), Mapping the dayside ionosphere to the magnetosphere according to particle precipitation characteristics, *Geophys. Res. Lett.*, *19*, 609, doi:10.1029/92GL00404.

Ogawa, Y., R. Fujii, S. C. Buchert, S. Nozawa, S. Watanabe, and A. P. van Eyken (2000), Simultaneous EISCAT Svalbard and VHF radar observations of ion upflows at different aspect angles, *Geophys. Res. Lett.*, *27*, 81, doi:10.1029/1999GL010665.

Ogawa, Y., R. Fujii, S. C. Buchert, S. Nozawa, and S. Ohtani (2003), Simultaneous EISCAT Svalbard radar and DMSP observations of ion upflow in the dayside polar ionosphere, *J. Geophys. Res.*, *108*(A3), 1101, doi10.1029/2002JA009590.

Otto, A., D. Lummerzheim, H. Zhu, Ø. Lie-Svendsen, M. H. Rees, and B. S. Lanchester (2003), Excitation of tall auroral rays by ohmic heating in field-aligned current filaments at F region heights, *J. Geophys. Res.*, *108*(A4), 8017, doi:10.1029/2002JA009423.

Oyama, K.-I., and T. Abe (1987), Anisotropy of electron temperature in the ionosphere, *Geophys. Res. Lett.*, *14*, 1195, doi:10.1029/GL014i012p01195.

Oyama, K.-I., and K. Schlegel (1988), Observation of electron temperature anisotropy in the ionosphere: A review, *Ann. Geophys.*, *6*, 389.

Oyama, K. I., K. Hirao, and F. Yasuhara (1985), Electron temperature probe on board Japan's 9th scientific satellite "OHZORA", *J. Geomagn. Geoelectr.*, *37*, 413.

Pollock, C. J., T. E. Moore, M. L. Adrian, P. M. Kintner, and R. L. Arnoldy (1996), SCIFER - Cleft region thermal electron distribution functions, *Geophys. Res. Lett.*, *23*, 1881, doi:10.1029/96GL01486.

Rees, M. H. (1989), *Physics and Chemistry of the Upper Atmosphere*, Cambridge Univ. Press, Cambridge, U. K.

Reigber, C., H. Lühr, and H. Schwintzer (2002), CHAMP mission status, *Adv. Space Res.*, *30*, 129.

Sadler, B., M. Lessard, E. Lund, A. Otto, and H. Lühr (2012), Auroral precipitation as a driver of neutral density enhancement in the cusp, *J. Atmos. Solar Terr. Phys.*, doi:10.1016/j.jastp.2012.03.003, in press.

Sandholt, P. E., C. S. Deehr, A. Egeland, B. Lybekk, R. Viereck, and G. J. Romick (1986), Signatures in the dayside cusp aurora of plasma transfer from the magnetosheath, *J. Geophys. Res.*, *91*, 10,063, doi:10.1029/JA091iA09p10063.

Sandholt, P. E., J. Moen, A. Rudland, D. Opsvik, W. F. Denig, and T. Hansen (1993), Auroral event sequences at the dayside polar cap boundary for positive and negative Interplanetary magnetic field B_Y, *J. Geophys. Res.*, *98*, 7737, doi:10.1029/92JA02256.

Semeter, J. (2003), Critical comparison of OII(732–733 nm), OI(630 nm), and N^2(1PG) emissions in auroral rays, *Geophys. Res. Lett.*, *30*(5), 1225, doi:10.1029/2002GL015828.

Strangeway, R. J. (2012), The equivalence of Joule dissipation and frictional heating in the collisional ionosphere, *J. Geophys. Res.*, *117*, A02310, doi:10.1029/2011JA017302.

Strangeway, R. J., R. E. Ergun, Y. J. Su, C. W. Carlson, and R. C. Elphic (2005), Factors controlling ionospheric outflows as observed at intermediate altitudes, *J. Geophys. Res.*, *110*, A03221, doi:10.1029/2004JA010829.

Tung, Y.-K., C. W. Carlson, J. P. McFadden, D. M. Klumpar, G. K. Parks, W. J. Peria, and K. Liou (2001), Auroral polar cap boundary ion conic outflow observed on FAST, *J. Geophys. Res.*, *106*, 3603, doi:10.1029/2000JA900115.

Watanabe, S., K.-I. Oyama, and T. Abe (1989), Anisotropic electron energy distribution in the topside ionospheric *F*-region, *Planet. Space Sci.*, *37*, 1207.

Yau, A. W., H. G. James, and W. Liu (2006), The Canadian Enhanced Polar Outflow Probe (e-POP) mission in ILWS, *Adv. Space Res.*, *38*, 1870, doi:10.1016/j.asr.2005.01.058.

Zettergren, M., J. Semeter, P.-L. Blelly, G. Sivjee, I. Azeem, S. Mende, H. Gleisner, M. Diaz, and O. Witasse (2008), Optical estimation of auroral ion upflow: 2. A case study, *J. Geophys. Res.*, *113*, A07308, doi:10.1029/2008JA013135.

Zhang, B.-C., Y. Kamide, and R.-Y. Liu (2003), Response of electron temperature to field-aligned current carried by thermal electrons: A model, *J. Geophys. Res.*, *108*(A5), 1169, doi:10.1029/2002JA009532.

Zheng, Y., T. E. Moore, F. S. Mozer, C. T. Russell, and R. J. Strangeway (2005), Polar study of ionospheric ion outflow versus energy input, *J. Geophys. Res.*, *110*, A07210, doi:10.1029/2004JA010995.

Zhu, H., A. Otto, D. Lummerzheim, M. H. Rees, and B. S. Lanchester (2001), Ionosphere-magnetosphere simulation of small-scale structure and dynamics, *J. Geophys. Res.*, *106*, 1795, doi:10.1029/1999JA000291.